Chapter 28: Iron Mineralogy, Oxidation State, and Alteration on Mars from Mössbauer Spectroscopy at Gusev Crater and Meridiani Planum

Richard V. Morris[1], Christian Schröder[2], Göstar Klingelhöfer[3], and David G. Agresti[4]

[1]Exploration and Integration Science Division,
NASA Johnson Space Center, Houston, TX, USA
[2]Biological and Environmental Sciences, University of Stirling, Stirling FK9 4LA, United Kingdom
[3]Institut für Anorganische und Analytische Chemie, Johannes Gutenberg-Universität, Mainz, Germany
[4]Department of Physics, University of Alabama at Birmingham, Birmingham, AL, USA

Abstract. Mössbauer instruments were included on the Mars Exploration Rover (MER) Mission to determine the mineralogical composition, diversity, and oxidation state of Fe-bearing igneous materials and alteration products. A total of 16 Fe-bearing phases (mutually consistent with bulk-sample chemistry) were identified, including Fe associated with the rock-forming minerals olivine, pyroxene, magnetite, ilmenite, and chromite and alteration products including Fe^{3+}-bearing oxyhydroxides (nanophase ferric oxide, hematite, and goethite) and sulfates (jarosite and an unassigned Fe^{3+} sulfate phase), and Fe^{2+} carbonate. Igneous rock types ranged from olivine-pyroxene and olivine-pyroxene-magnetite basalts to ultramafic rocks at Gusev Crater. Jarosite-hematite bedrock was pervasive at Meridiani Planum, and concretions winnowed from the outcrop were mineralogically hematite. Because their structures contain hydroxyl, goethite and jarosite provide mineralogical evidence for aqueous processes on Mars, and jarosite and Fe^{3+}-sulfate are evidence for acid-sulfate processes at both Gusev Crater and Meridiani Planum. A population of rocks on the Meridiani Planum outcrop was identified as iron and stony meteorites by the presence of Fe metal (kamacite) and the sulfide troilite. The MER mission demonstrates that Mössbauer spectrometers landed on any Fe-bearing planetary surface provide first-order information on igneous provinces, alteration state, and alteration style and provide well-constrained criteria for sample selection on planetary sample-return missions including planets, moons, and asteroids.

28.1 Introduction and Background

The Mars Exploration Rover (MER) named "*Spirit*" landed on the plains of Gusev Crater on 4 January, 2004, and its twin "*Opportunity*" landed on the opposite side of the planet at Meridiani Planum on 24 January 2004 (Squyres *et al.*, 2004a, 2004b). Both MER rovers carried the Athena science instrument package (Squyres *et al.*, 2003) which included a miniature Mössbauer (MB) spectrometer MIMOS II (Klingelhöfer *et al.*, 2003). The instrument detects only ^{57}Fe (~2% of natural Fe), and peak positions in MB spectra constrain Fe speciation according to oxidation (e.g., Fe^0, Fe^{2+}, and Fe^{3+}) and coordination (e.g., tetrahedral and octahedral) states and mineralogy of Fe-bearing phases. Peak areas provide quantitative information on the relative distribution of Fe among Fe-bearing phases and oxidation and coordination states.

In a remote sensing environment, Mössbauer spectra provide geochemical and mineralogical information that is not readily obtained by other methods. Primary igneous rocks are normally dominated by Fe^{2+} (e.g., olivine, pyroxene, ilmenite, magnetite, and chromite) and secondary alteration products are normally dominated by Fe^{3+} (e.g., oxides and oxyhydroxides, sulfates, and amorphous materials), so that the parameter $Fe^{3+}/\Sigma Fe$ is a first-order measure of the alteration state of primary igneous material. The actual situation is more complex, because some minerals can be primary or secondary and can have both Fe^{2+} and Fe^{3+} (e.g., magnetite Fe_3O_4) and some secondary alteration products are predominantly Fe^{2+} (e.g., siderite $FeCO_3$). Thus to determine the extent and style of alteration, the redox information and Fe phase assignments must be considered together. The style of alteration (e.g., hydrolytic versus sulfatic) is inferred by phase assignment of Fe-bearing alteration products.

In this chapter, we describe the functionality of the MER MB instrument and summarize the salient Mössbauer results obtained at Gusev Crater and Meridiani Planum where 155 and 114 MB spectra were acquired, respectively. *Spirit's* mission at Gusev Crater ended on sol 2210 with the last MB spectrum acquired on sol 2071. A sol is one martian day with landing day sol 0. *Opportunity's* mission is ongoing as of June, 2017, but MB spectra were not acquired after sol 2871 because the low ^{57}Co source intensity at that point required unacceptably long integration times. Mission overview papers relevant to Mössbauer activity are published by Squyres *et al.* (2006, 2009), Arvidson *et al.* (2006, 2008, 2010a, 2010b), and Ashley *et al.* (2011).

28.2 Instrument and Methods

For a full discussion of the Mössbauer effect and Mössbauer spectroscopy, the reader is referred to the literature (e.g., Bancroft, 1973; Hawthorne, 1988; Burns, 1993; Gütlich *et al.*, 2011; Gütlich and Schröder, 2012; Yoshida and Langouche, 2013; Dyar and Sklute, 2018). Most laboratory MB spectrometers employ transmission geometry where the sample is located between the ^{57}Co source and the detector. For a planetary surface mission involving in situ measurements, the MER MIMOS II instruments (Klingelhöfer *et al.*, 2003) employed instead backscatter geometry (source and detector are on the same side of the sample) because no sample preparation is required (Figure 28.1). To acquire a MIMOS II spectrum (emitted counts versus source velocity in units of mm/s) for a martian surface target (rock or soil), the instrument's sensor head was placed in physical contact with the target by the rover's robotic arm (Figure 28.2). The ^{57}Co source activity at landing was ~150 mCi and <1 mCi when acquisition of MB spectra ceased. Martian MIMOS II spectra were acquired in temperature intervals 10 K wide during real-time temperature binning using the temperature sensor on the MB contact plate in order to detect temperature dependent changes in MB spectra. The MER instruments are configured with an internal standard (α-Fe metal foil) and an additional detector in order to simultaneously acquire a α-Fe metal transmission MB spectrum for each surface target (Klingelhöfer *et al.,* 2003).

Peak positions in MB spectra are described by the center shift (δ in mm/s) relative to zero velocity taken as the center point of the spectrum of α-Fe metal foil (standard practice), the quadrupole splitting (ΔE_Q in mm/s), and (for sextets) the magnetic hyperfine field (B_{hf} in T). These parameters for MER targets were, in most cases, calculated from spectra that are the sum of all individual temperature channels for the emitted 14.4 keV γ-rays (to maximize counting statistics). To investigate temperature dependence of parameters, spectra from individual temperature channels are summed over spectra acquired at different locations exhibiting similar

mineral composition. MIMOS II integrations were acquired during the nighttime nominally between ~200 K and ~270 K (with 235 ± 15 K taken as the median temperature).

Because, in our application, the reference α-Fe foil and martian surface targets are at the same temperature, the values obtained for δ may be directly compared with databases complied from measurements made with source and absorber at ambient laboratory temperatures (e.g., Burns and Solberg, 1990; Burns, 1993; McCammon, 1995; Stevens *et al.*, 1998). However, both ΔE_Q and B_{hf} may exhibit a temperature dependence, which if significant would require either a database obtained on samples measured at the same temperatures as the MER targets or extrapolation of MER results to laboratory temperatures based on the temperature variation observed by the MER instruments.
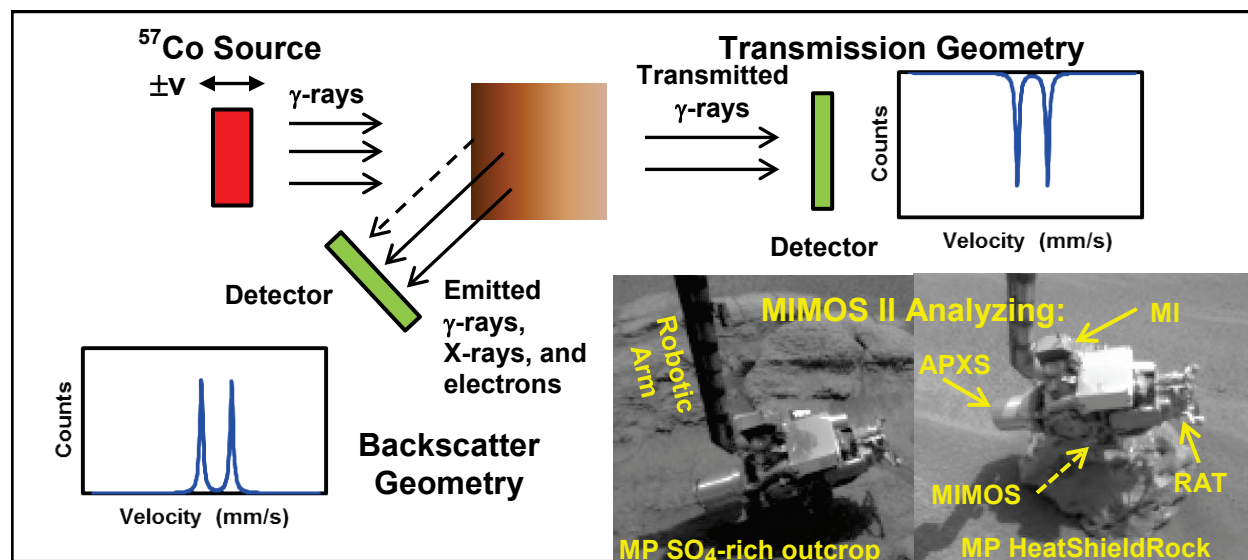

Figure 28.1. Measurement geometry for Mössbauer spectrometers. In transmission geometry, sample (absorber) is between nuclear source (^{57}Co/Rh; 14.4 keV) and detector(s), peaks are negative features, and the sample should be thin with respect to absorption of γ-rays to minimize non-linear effects. In backscatter geometry, source and detector are on the same side of the sample, peaks are positive features corresponding to recoilless emission of γ-rays, internal conversion X-rays, and electrons. MIMOS II instruments employ backscatter geometry and simultaneously detect emitted 14.4 keV γ-rays and ~6.4 keV X-rays. MIMOS spectra are counts per velocity channel as a function of velocity in units of mm/s relative to the midpoint of the spectrum of α-Fe^0 which is obtained from an internal standard. Modified after Klingelhöfer et al. (2003). Inset: Front Hazcam images show MIMOS II acquiring data on Meridiani Planum (MP) SO$_3$-rich outcrop (left, sol 31B image 1F130936200EDN0454P1131L0M1-BR) and HeatShieldRock (right, sol 350B image 1F159253265EDN40DPP1131L0M1-BR). The MIMOS instrument is hidden from view by other robotic arm instruments. APXS = Alpha Particle X-Ray Spectrometer; MI = Microscopic Imager; RAT = Rock Abrasion Tool.

Mössbauer parameters calculated from MIMOS II spectra reported in Morris *et al.* (2006a, 2006b), and in all subsequent publications by the MER Mössbauer instrument team, are based on a refinement of the velocity calibration employed in the two initial MER Mössbauer

publications (Morris *et al.*, 2004; Klingelhöfer *et al.*, 2004). This refinement included the temperature dependence of B_{hf} for the α-Fe metal foil standard (Morris *et al.*, 2006b). Therefore, comparisons of laboratory measurements with MER results should be based on data in MER publications from 2006 and beyond. Morris *et al.* (2006a, 2006b) report for the Fe^{3+} doublets of npOx, jarosite, and Fe3D3 that their values of ΔE_Q are temperature independent over the measurement interval on the martian surface, so that the average values at 235 ± 15 K are the same within uncertainty (± 0.02 mm/s) as the values obtained by extrapolation to ambient terrestrial ambient temperatures. The same relationship held for Fe^{2+} doublets assigned to pyroxene, but a weak temperature dependence is indicated for Fe^{2+} doublet assigned to olivine (martian-surface average and ambient-terrestrial extrapolated values are 2.99 ± 0.03 mm/s and 2.94 ± 0.03 mm/s, respectively).
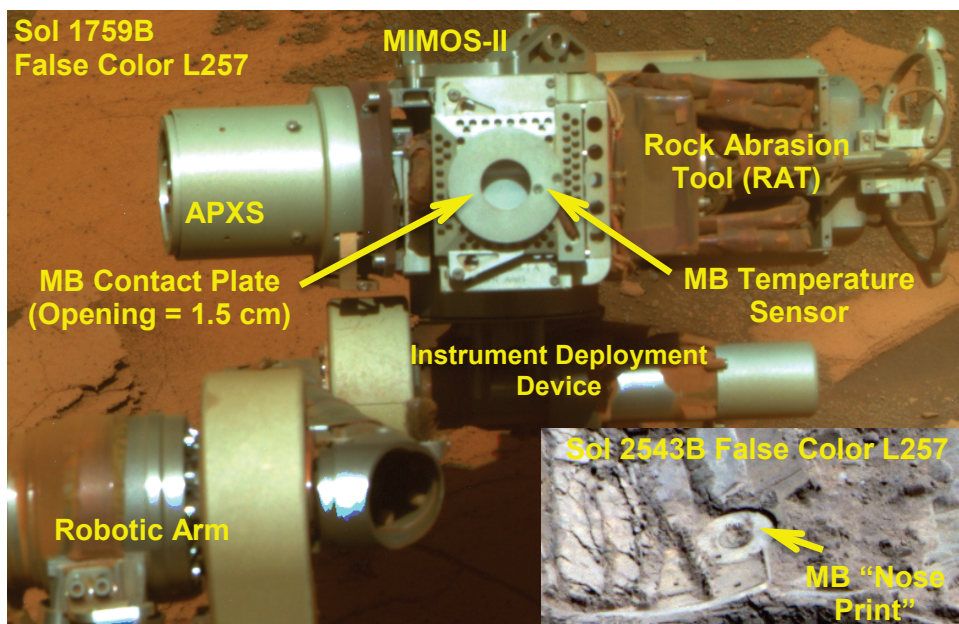

Figure 28.2. False color image of the MIMOS II Mössbauer spectrometer mounted on Opportunity's Instrument Deployment Device. Hole in MB contact plate (1.5 cm diameter) defines the field of view. Contact plate has a sensor for measurement of surface temperatures. Inset shows "nose print" of contact plate made during analysis of soil in a trench made by the churning action of rover wheels.

MB spectra are linear sums of subspectra from all distinct Fe sites (i.e. distinct sites relative to oxidation and coordination states and mineralogical speciation). For mineralogical speciation, MB provides quantitative data on the relative distribution of total Fe among Fe-bearing phases but does not provide information on absolute abundances of Fe-bearing phases themselves unless the concentration of Fe in those phases is known or can be estimated. McSween *et al.* (2008) provide a template for deriving such estimates. Subspectral areas (A), which here are the sum of peak areas associated with each Fe- bearing phase, and their defining MB parameters (δ, ΔE_Q, field B_{hf}) were obtained by least squares fitting procedures (see Morris *et al.*, 2006a, 2006b). Subspectral areas include a correction factor that accounts for recoil-free fraction differences between Fe oxidation states ($f(Fe^{3+})/f(Fe^{2+}) = 1.21$) (De Grave and Van Alboom, 1991; Morris *et al.*, 1995). In general, MER MB spectra are characterized by multiple

occurrences of the same Fe-bearing phases present in different proportions. This repetition aided in Fe speciation assignments and provided fitting constraints (e.g., constrain all MB parameters except subspectral areas) late in the mission when low source intensities resulted in MB spectra with poor counting statistics.

MIMOS II can "see through" thin layers of dust and provide mineralogical information about underlying surfaces. From laboratory measurements detecting the 14.4 keV radiation, a layer of air-fall basaltic dust more than ~3 mm thick will fully mask underlying surfaces from detection (Morris *et al.*, 2001a, 2001b; Graff *et al.*, 2001; Klingelhöfer *et al.*, 2003). According to the authors, the dust layer is characterized by particle diameters ≤10 μm, and the palagonitic tephra used as the dust source (<1 mm size fraction) has total Fe concentrations equal to 15.49 wt.% and 22.33 wt.% for the <1 mm and <5 μm size fractions, respectively.

28.3 Mineralogical Assignment of Fe-Bearing Phases

Sixteen Fe-bearing phases, mutually consistent with APXS chemistry, were identified at Gusev Crater and Meridiani Planum (Figure 28.3) (Morris *et al.*, 2006a, 2006b, 2008, 2010, 2018). The most frequent and coupled detections at Gusev Crater, and also common at Meridiani Planum, are Fe^{2+} in olivine ((Fe^{2+},Mg)$_2$SiO$_4$) and pyroxene ((Fe^{2+},Mg,Ca)SiO$_3$) from primary igneous minerals and Fe^{3+} in npOx (nanophase ferric oxide). Ferrous iron in olivine was misassigned to hydrous iron sulfate by Lane *et al.* (2004) (Morris *et al.*, 2006). NpOx is a generic name for doublet alteration products having octahedrally coordinated Fe^{3+} and includes any combination of a number of phases like ferrihydrite, hisingerite, schwertmannite, akaganeite, and superparamagnetic hematite and goethite. Other Fe-bearing igneous minerals found by MB at Gusev Crater together with olivine and pyroxene are multiple detections of magnetite (Fe^{3+}($Fe^{2+}Fe^{3+}$)O$_4$) and ilmenite (Fe^{2+}TiO$_3$) and a singular detection of chromite (Fe^{2+},Fe^{3+},Mg,Al)Cr$_2$O$_4$). All other Fe-bearing phases at Gusev Crater with two exceptions are the Fe^{3+} alteration products hematite (α-Fe$_2$O$_3$), goethite (α-FeOOH), and ferric sulfate. We have not made specific mineralogical assignments for ferric sulfate because its Mössbauer parameters are not mineralogically specific and have adopted the generic nickname "Fe3Sulfate". Possible assignments consistent with other MER data include ferricopiapite, rhomboclase, and amorphous ferric sulfate (Lane *et al.*, 2008; Dyar *et al.*, 2013; Morris *et al.*, 2017) but not the hydroxy sulfate jarosite (discussed below). The two exceptions are singular detections of pyrite/marcasite (FeS$_2$) and Fe^{2+}-bearing carbonate (Fe^{2+},Mg,Ca)CO$_3$.

Lane *et al.* (2008) and Hausrath *et al.* (2013) have suggested that certain ferric phosphates could contribute in part to the Fe3Sulfate doublet at the Paso Robles location. While the relative proportions of phosphate versus sulfate is equivocal for MB measurements of targets PasoRobles and PasoLight1, P$_2$O$_5$ concentrations for Inner Basin and Home Plate targets (e.g., AradSamra) are insufficient for ferric phosphates to make a significant contribution to Fe3Sulfate (Dyar *et al.*, 2014; Morris *et al.*, 2017).

The most frequent detections at Meridiani Planum are Fe^{3+} assigned to jarosite (K,Na,H$_3$O)Fe$_3$(OH)$_6$(SO$_4$)$_2$, hematite, and an unassigned Fe^{3+}-bearing phase nicknamed "Fe3D3", and they occur together in the SO$_3$-rich bedrock. The uniqueness of the jarosite assignment was questioned by Dyar *et al.* (2013), but their interpretation was based on the velocity calibration of Klingelhöfer *et al.* (2004) rather than the revised calibration (Morris *et al.*, 2006b) employed thereafter. The MB parameters for Fe3D3, Fe3Sulfate, and npOx are not mutually exclusive but do not generally overlap (Figure 28.3), implying distinct Fe^{3+} speciation

5

associated with different provenances (sulfate-bearing outcrop, sulfate-bearing soil, and basaltic soil and rock, respectively). Fleischer *et al.* (2010a) suggest a continuum of hematite particle diameters is present, with coarse represented by the hematite concretions, intermediate represented by outcrop hematite with sextet subspectra, and fine by the Fe3D3 doublet interpreted as superparamagnetic hematite. The concretions ("blueberries") are imbedded in the SO_3-rich outcrop and occur as discrete spherules admixed with, and as lag upon, basaltic soil. The remaining Fe mineralogical assignments, Fe^0 in kamacite (a low-Ni Fe/Ni alloy) and the Fe-sulfide troilite (FeS), are all associated with meteorites identified on the surface of the SO_3-rich outcrop at Meridiani Planum. Some combination of Fe-carbide cohenite (Fe_3C) and Fe-phosphide schreibersite $(Fe,Ni)_3P$ may also be present, but are considered tentative identifications because their aggregate concentration is at detection limits.
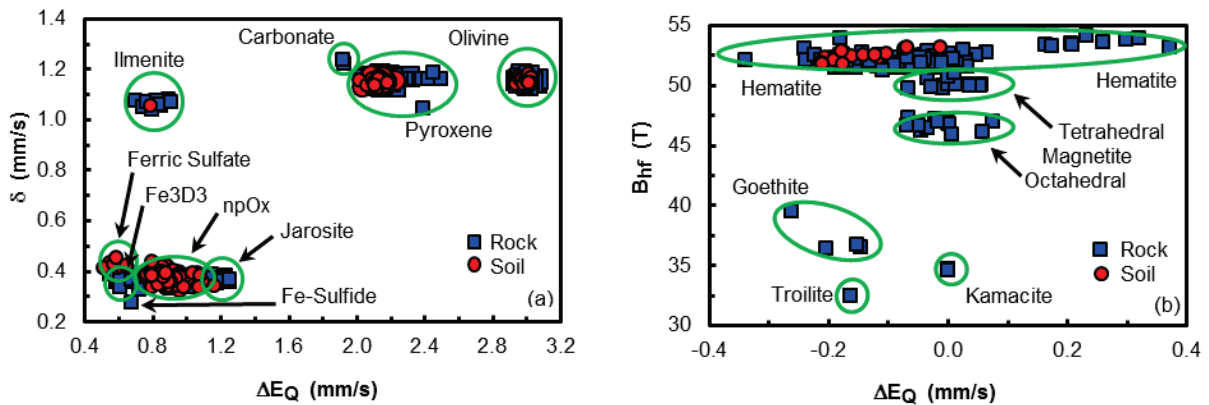

Figure 28.3. MIMOS II phase identification diagrams (235 ±15 K) (a) Center shift (δ) versus quadrupole splitting (ΔE_Q) for doublet subspectra aside from chromite. Ilmenite, carbonate, pyroxene, and olivine are Fe^{2+} bearing phases. Ferric sulfate, Fe3D3, npOx, and jarosite are Fe^{3+}-bearing phases. Fe-Sulfide is FeS_2 (pyrite/marcasite). (b) Hyperfine field strength (B_{hf}) versus ΔE_Q for sextet subspectra. Hematite and goethite are Fe^{3+} phases, magnetite is a Fe^{2+}-Fe^{3+} phase with distinct tetrahedral (Fe^{3+}) and octahedral (Fe^{2+},Fe^{3+}) sites, troilite is an FeS sulfide, and kamacite is a Fe-Ni alloy (~5% Ni). Mössbauer velocity calibration after Morris et al. (2006a, 2006b).

28.4 Mössbauer Mineralogy and Fe Oxidation State of Rocks and Soils

28.4.1 Scope

Our purpose is to summarize mineralogical composition and redox state of rocks and soils and their distributions across the MER landing sites at Gusev Crater and Meridiani Planum. Encompassed are all MB results from Gusev Crater and all those through sol 557 and a few thereafter for Meridiani Planum. The MB results alone provide first-order information concerning identification and mineralogical variability of igneous rocks and equivalent information about non-igneous rocks. We take unaltered to weakly altered basaltic rock and soil to have >75 % of their total Fe associated with olivine, pyroxene, ilmenite, chromite, magnetite, kamacite and troilite (i.e., $Fe_{igneous} \equiv Ol + Px + Ilm + Chr + Mt + Kam + Tr > 75$ %). The magnitudes of $Fe_{igneous}$ and $Fe^{3+}/\Sigma Fe$ are shown in Figure 28.4 as a function of sol number as a surrogate for physical rover location. Note that even for wholly igneous rocks, $Fe^{3+}/\Sigma Fe$ can vary

in accordance with the magnetite content ($Fe^{3+}/\Sigma Fe = 0.67$ for stoichiometric magnetite). Nevertheless, the magnitude of $Fe^{3+}/\Sigma Fe$ provides a quantitative measure on the extent of oxidative alteration, and the associated mineralogical compositions of Fe^{3+}-bearing phases (e.g., hematite, goethite, and Fe^{3+}-sulfate) constrain the alteration style.
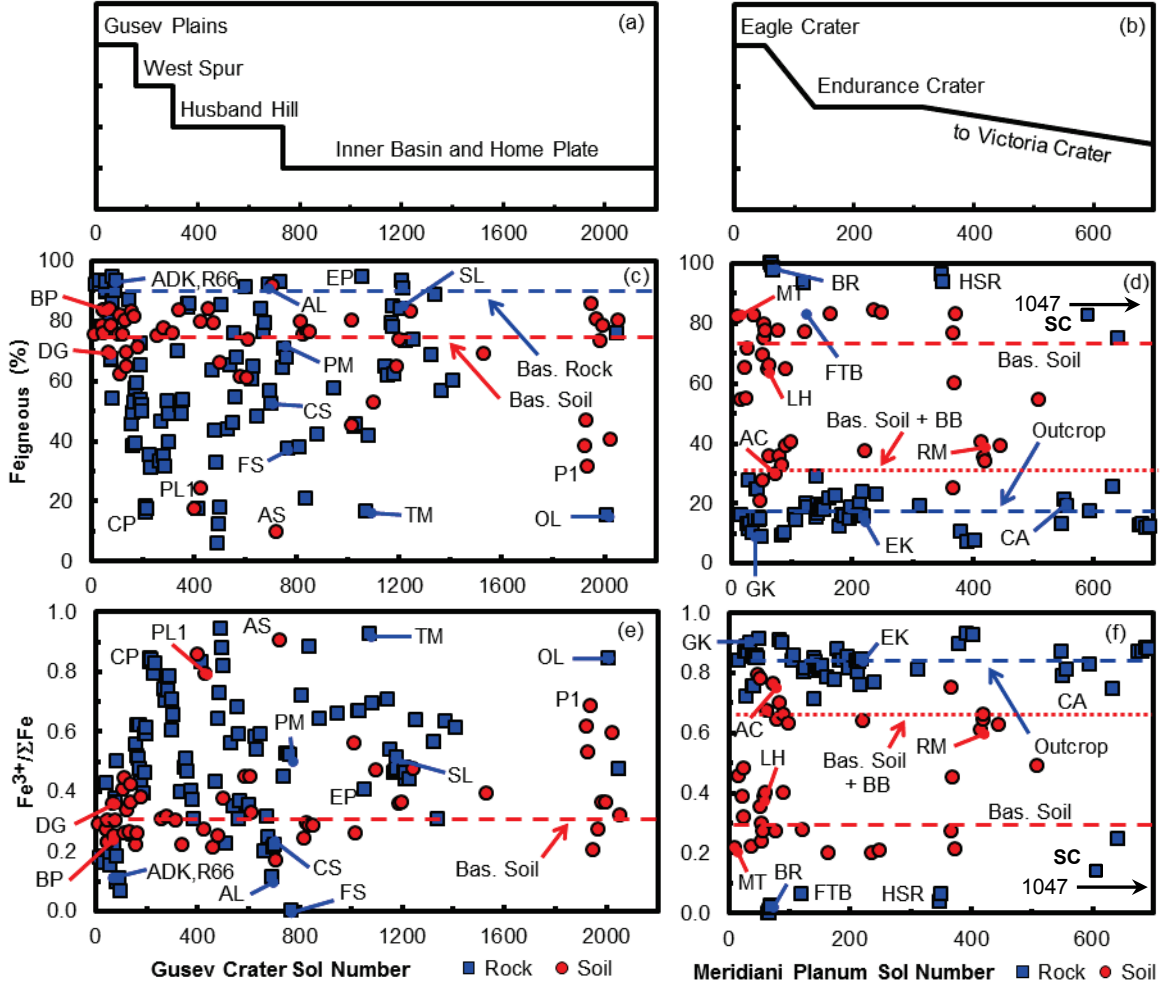

Figure 28.4. Physical location (a and b), $Fe_{igneous}$ (c and d), and $Fe^{3+}/\Sigma Fe$ (e and f) as a function of sol number for analysis targets at Gusev Crater (a, c, and e) and Meridiani Planum (b, d, and f). $Fe_{igneous} \equiv Ol + Px + Ilm + Chr + Mt + Kam + Tr$ (see text); BB = hematite concretions (blueberries). Subspectral areas and key to target names are given in Table 28.1. Locations from Arvidson et al. (2006, 2008).

Subspectral areas and values of $Fe_{igneous}$ and $Fe^{3+}/\Sigma Fe$ are compiled in Table 28.1 for the representative MB targets named in Figure 28.4, and MB spectra for specific targets are plotted in Figures 28.5 and 28.6 for Gusev Crater and in Figure 28.7 for Meridiani Planum. The discussion that follows for Gusev Crater is based on publications by Morris *et al.* (2004, 2006a, 2008, 2010, 2017), Klingelhöfer *et al.* (2005), Yen *et al.* (2005, 2008), Clark *et al.* (2007), Morris and Klingelhöfer (2008), and Squyres *et al.* (2008). Relevant publications for Meridiani Planum are Klingelhöfer *et al.* (2004), Morris *et al.* (2006b, 2017), Clark *et al.* (2005), Morris and Klingelhöfer (2008), Fleischer *et al.* (2010a, 2010b, 2011), Schröder *et al.* (2008, 2010, 2016), and Zipfel *et al.* (2011).

Table 28.1. *Sol number, target type, target surface state, subspectral areas, Fe^{3+}/ΣFe, and Fe$_{igneous}$ for representative targets from Gusev Crater and Meridiani Planum.*

Target	Sol	Type	Sur-face	Ol (%)	Px (%)	Mt (%)	npOx (%)	Hm (%)	Other Phase	(%)	Fe^{3+}/ΣFe	Fe$_{igneous}$ (%)	Key
						Gusev Crater							
Adirondack	34	R	R	48	32	13	6	---	---	---	0.29	94	ADK
DesertGobi	69	S	U	30	33	7	28	2	---	---	0.36	70	DG
BearPawPanda	73	S	D	37	35	12	13	3	---	---	0.25	84	BP
Route66	100	R	B	57	37	---	7	---	---	---	0.07	93	R66
ClovisPlano	218	R	R	1	14	2	25	18	Gt	40	0.84	17	CP
PasoLight1	421	S	D	10	8	6	---	7	Fe3Sulfate	69	0.86	24	PL1
AlgonquinIroquet	690	R	B	71	13	6	8		Ilm	2	0.11	92	AL
ComancheSpur	702	R	B	51	---	1	16	5	Carb	27	0.22	52	CS
AradSamra	723	S	D	7	3	---	---	4	Fe3Sulfate	86	0.90	10	AS
PoseyManager	754	R	B	17	23	31	27	3	---	---	0.53	70	PM
FuzzySmith	769	R	U	4	26	---	---	---	Ilm / FeS2	8 / 63	0.00	30	FS
EsperanzaPalma	1056	R	U	---	4	45	4	1	---	---	0.40	95	EP
TrollMontalva	1073	R	U	---	3	14	5	78	---	---	0.93	17	TM
ExamineThisSlide	1177	R	B	4	33	41	22	---	---	---	0.51	78	SL
TroyPenina1	1937	S	D	15	17	---	---	---	Fe3Sulfate	68	0.68	32	P1
TroyOliveLeaf	2000	R	U	6	9	---	---	---	Fe3Sulfate	85	0.85	15	OL
						Meridiani Planum							
MerlotTarmack	11	S	U	39	37	6	14	4	---	---	0.22	82	MT
GuadalupeKing3	35	R	R	1	9	---	---	36	Jar / Fe3D3	38 / 16	0.90	10	GK
MtBlancLesHauche	60	S	U	28	32	5	30	5	---	---	0.39	65	LH
BounceRockCase	69	R	R	---	100	---	---	---	---	---	0.00	100	BR
SeasAegeanCrest	73	S	U	11	12	8	5	65	---	---	0.76	31	AC
FigTreeBarberton2	121	R	U	48	32	---	6	---	Kam / Tr	11 / 3	0.06	94	FTB
EscherKirchner	219	R	R	1	15	---	---	35	Jar / Fe3D3	30 / 20	0.84	16	EK
HeatShieldRock	351	R	B	---	---	---	6	---	Kam	94	0.06	94	HSR
MattsRippleMobarak	415	S	U	17	21	2	11	48	---	---	0.61	40	RM
CobblesArkansas	551	R	U	6	15	---	52	8	Jar	19	0.79	21	CA
SantaCatarina	1047	R	U	52	26	---	14	---	Kam / Tr	1 / 6	0.13	85	SC

Notes: (1). Type: R = rock; S = soil. (2). Surface state for rocks: U = undisturbed surface; B = brushed surface; R = surface removed with Rock Abrasion Tool. (3). Surface state for soils: U = undisturbed surface; D = surface disturbed by rover wheels. (4). Subspectral areas (corrected for recoil-free fractions; see text): Ol = Fe^{2+} associated with olivine; Px = Fe^{2+} associated with pyroxene; Ilm = Fe^{2+} associated with ilmenite; Mt = Fe^{2+} and Fe^{3+} associated with magnetite; Chr = Fe^{2+} and Fe^{3+} associated with chromite; npOx = Fe^{3+} associated with nanophase ferric oxide; Hm = Fe^{3+} associated with hematite; Gt = Fe^{3+} associated with goethite; Carb = Fe^{2+} associated with carbonate; Fe3Sulfate = Fe^{3+} associated with unassigned doublet sulfate phase; FeS2 = Fe-sulfide associated with pyrite/marcasite; Kam = Fe^{0} associated with Fe metal alloy with ~5 wt.% Ni; Jar = Fe^{3+} associated with jarosite; Fe3D3 = Fe^{3+} associated with unassigned doublet phase at Meridiani Planum; Tr = Fe associated with troilite. (5). Fe$_{igneous}$ = Ol + Px +Ilm + Mt + Chr + Kam + Tr. (6). Formally SpongeBobSquidward but popularly known as HeatShieldRock. Kamacite for HSR includes minor contributions from cohenite and/or schreibersite.

28.4.2 Gusev Crater

Basaltic rocks (Fe$_{igneous}$ >75%) are prevalent at the Gusev Crater landing site (Figure 28.4). Olivine-rich basaltic rocks are common on the Gusev plains (e.g., Route66; Figure 28.5a), and magnetite-rich basaltic rocks with relatively more Fe^{2+} in pyroxene and less in olivine are common in the Columbia Hills at West Spur, Husband Hill, and Home Plate (e.g.,

PoseyManager and Slide; Figure 28.5b and 28.5c). Basaltic soil (Figure 28.5d) at Gusev Crater is most akin to rock Route66 and similar rocks (e.g., Adirondack and Humphrey) on the Gusev plains, implying the abundance of that mineralogical combination across Mars as opposed to magnetite-rich assemblages. Rocks with ultramafic Fe^{2+} mineral assemblages (olivine dominant) were analyzed on Husband Hill (e.g., Algonquin; Figure 28.5e), and just downslope *Spirit* analyzed outcrop with Fe^{2+}-bearing carbonate (Figure 28.5f). The ComancheSpur outcrop is the only carbonate-bearing target detected by the MER rovers.

Figure 28.5. Mössbauer spectra for Gusev Crater basaltic rocks (a) Route66, (b) PoseyManager, and (c) Slide, (d) basaltic soil DesertGobi, (e) ultramafic rock Algonquin, and (f) Fe^{2+}-bearing carbonate rock ComancheSpur. TC/BC = (Total Counts)/(Baseline Counts); GP = Gusev plains; HP = Home Plate; HH = Husband Hill.

The dominant Fe^{3+} alteration product on the Gusev plains is npOx. Its concentration is highly variable in basaltic soil (e.g., 13 % to 28 % for BearPawPanda and DesertGobi, respectively; Table 28.1), and npOx is also associated with basaltic dust. The dust coats rock surfaces, decreasing $Fe_{igneous}$ when the dust coating is not effectively removed by brushing or

9

abrasion by the Rock Abrasion Tool (RAT). Consistent with the assignment of the npOx ferric doublet to that phase and not, for example, an assignment to an igneous phase, is its correlation with the concentrations of SO_3 and Cl.

Highly altered rocks with goethite (detected only in rocks), hematite, and npOx (not associated with dust) as Fe^{3+}-bearing alteration products (e.g., WS_ClovisPlano; Figure 28.6a) were found at West Spur and Husband Hill. At West Spur and Home Plate, the churning action of *Spirit's* wheels revealed, just beneath the surface, light-toned soil with Fe^{3+}-bearing sulfate as the dominant Fe-bearing phase (e.g., HH_PasoLight1 and HP_AradSamra; Figure 28.6b). Fe^{3+}-bearing sulfate was detected only in soil with the exception of a small piece of crust (i.e., cemented soil). In close physical association with the Fe^{3+}-bearing sulfate soils at Home Plate are outcrops where the dominant Fe^{3+}-bearing alteration product is hematite (e.g., HP_Montalva; Figure 28.6c). A singular detection of pyrite-marcasite (FeS_2) was the float rock FuzzySmith (Figure 28.6d) located at Home Plate. The Home Plate structure itself is considered to be a fumarolic, acid-sulfate environment where Fe^{3+}-bearing sulfates are precipitation products of leachate solutions derived from (presumably local) basaltic progenitors. Co-located hematite is interpreted as a primary precipitate, possibly under hydrothermal conditions, or as a diagenetic alteration product of Fe^{3+}-bearing sulfates.
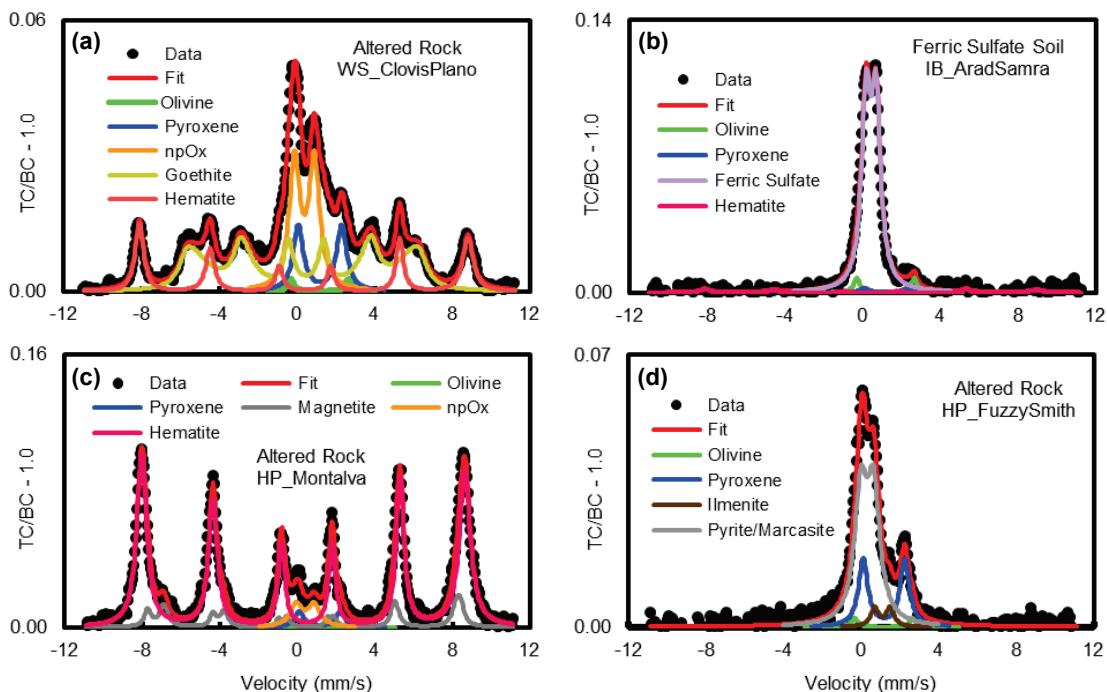

Figure 28.6. Mössbauer spectra for Gusev Crater (a) highly-altered rock WS_ClovisPlano, (b) Fe^{3+}-bearing sulfate soil IB_AradSamra, (c) hematite-rich outcrop HP_Montalva, and (d) pyrite/marcasite-bearing float rock HP_FuzzySmith. TC/BC = (Total Counts)/(Baseline Counts); WS = West Spur; IB = Inner Basin;. HP = Home Plate.

28.4.3 Meridiani Planum

Mössbauer measurements at Meridiani Planum are dominated by analyses of the SO_3-rich and jarosite-bearing bedrock, with average $Fe_{igneous}$ ~17 % and $Fe^{3+}/\Sigma Fe$ ~0.85 (Figure 28.4d and 28.4f). The Mössbauer data in the figure refer to outcrop matrix and do not include contributions

from imbedded hematite concretions (a.k.a. blueberries). The Fe mineralogy of the outcrop matrix (Figure 28.7a) is approximately subequal proportions of Fe^{3+} associated with jarosite $(H_3O,Na,K)Fe_3(SO_4)_2(OH)_6$), hematite, and an unassigned Fe^{3+}-bearing phase (Fe3D3), possibly superparamagnetic hematite. Soils are either basaltic (Figure 28.7b) or are mechanical mixtures of basaltic soil and hematite concretions winnowed from the outcrop. Basaltic soil MtBlancLesHauche has high proportions of npOx and is very similar to DesertGobi at Gusev Crater with respect to mineralogical composition (Table 28.1). The concretions tend to be concentrated as lag deposits on ripple crests (Figure 28.7c). No soil mineralogically equivalent to the outcrop was found, and no outcrops with basaltic mineralogical compositions were analyzed by Mössbauer while the instrument was operational. The Mössbauer detection of jarosite was particularly important because the mineral precipitates from aqueous acid sulfate solutions (pH <3-4), implying that the outcrop is the product of acid-sulfate alteration of basaltic progenitors.
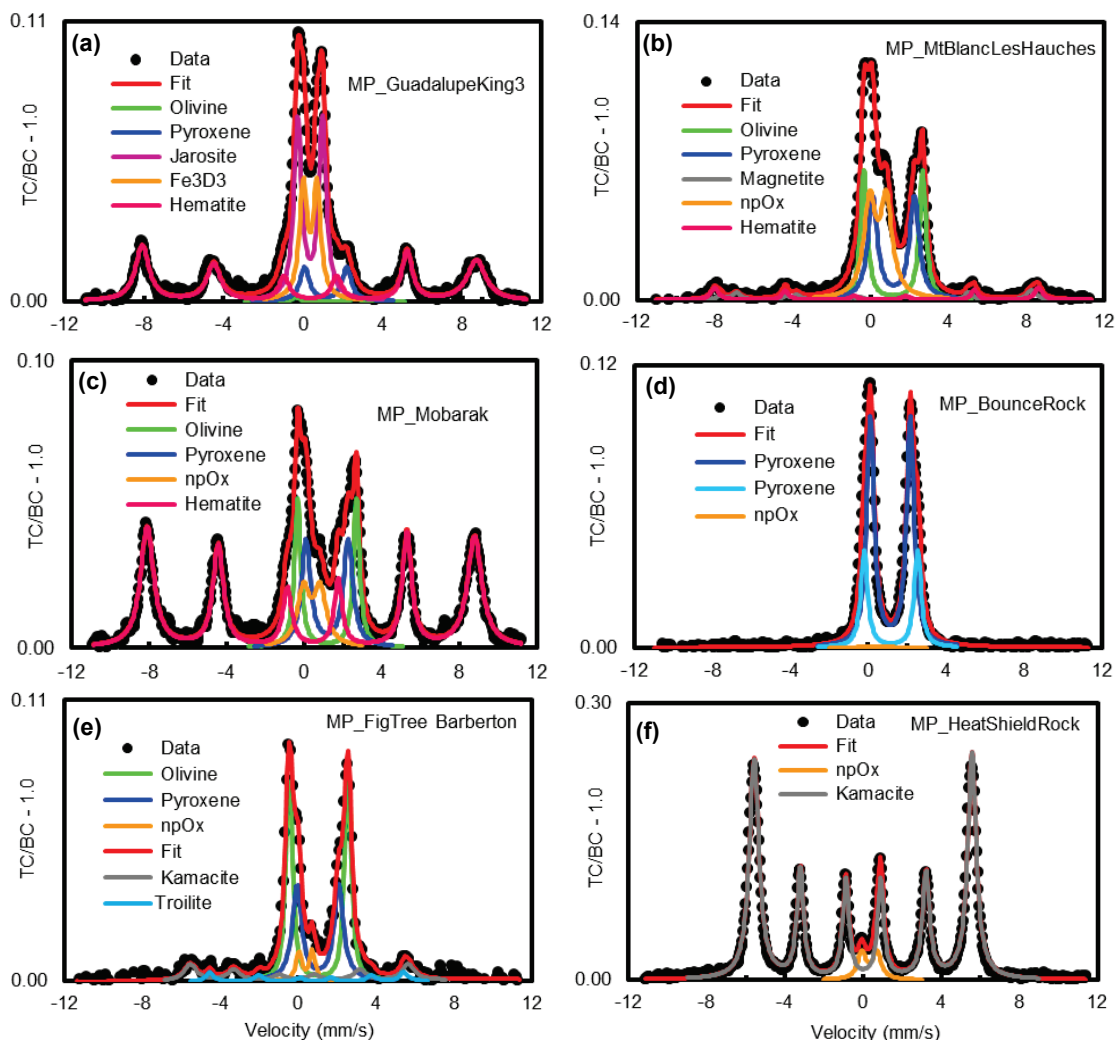

Figure 28.7. Representative Mössbauer spectra for Meridiani Planum (a) sulfate-rich bedrock matrix, (b) basaltic soil MontBlancLesHauches, (c) basaltic soil with hematite concretions (blueberries) as a ripple-crest lag deposit, (d) impact ejecta BounceRock, (e) stony meteorite FigTreeBarberton, and (f) iron meteorite HeatShieldRock. TC/BC = (Total Counts)/(Baseline Counts); MP = Meridiani Planum.

11

Float rocks ranging from pebble to boulder size (referred to as cobbles) were analyzed by MB on the surface of the SO$_3$-rich and jarosite-bearing bedrock and were interpreted as impact ejecta (e.g., BounceRock; Figure 28.7d), impact breccia (e.g., CobblesArkansas), stony meteorites (e.g., FigTreeBarberton; Figure 28.7e), and iron meteorites (e.g., HeatShieldRock; Figure 28.7f). Interestingly, BounceRock is, chemically and mineralogically, a Shergottite-like basalt. The Mössbauer detection of kamacite and/or troilite firmly established that cobbles like FigTreeBarberton are in fact stony meteorites on the martian surface and not indigenous basaltic rocks. Furthermore, the chemical and mineralogical similarity of FigTreeBarberton, SantaCatarina, Santorini, and Kasos implies that they are paired meteorites and possibly fragments of the impactor that created Victoria Crater.

28.5 Seeing Through the Dust on Mars

The Rock Abrasion Tool (RAT) was designed to brush rock surfaces relatively free of airfall dust and saltating soil particles and to grind into rock surfaces to remove this material and also sufficiently-thin "alteration" rinds in order to analyze "pristine" surfaces beneath. Because of the significant mineralogical and chemical contrast between basaltic soil (high Fe$_{igneous}$ and low SO$_3$ concentration) and the outcrop (low Fe$_{igneous}$ and high SO$_3$), measurement of RATed and undisturbed outcrop surfaces at Meridiani Planum are ideal for demonstrating "contamination" of the mineralogy and chemistry of rock surfaces by basaltic air-fall dust and saltating particles with respect to measurements by MB and APXS instruments.
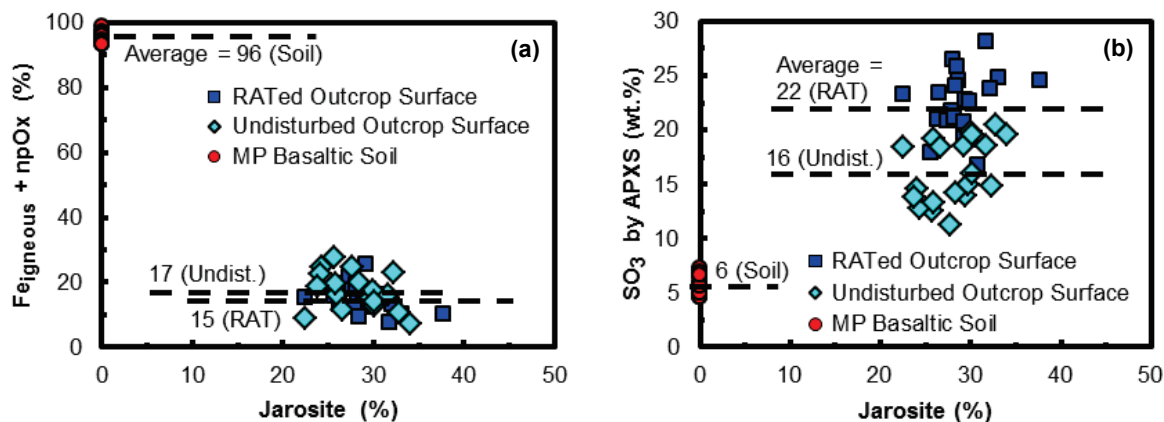

Figure 28.8. (a) Percentage of total Fe present as Fe$_{igneous}$ + npOx and (b) SO$_3$ concentration from APXS as a function the percentage of total Fe present as jarosite for Meridiani Planum (MP) basaltic soil and undisturbed and RATed outcrop rock surfaces. RAT = Rock Abrasion Tool.

Figure 28.8a is a binary plot using data derived from only MB measurements (14.4 keV emitted γ-rays). The y-axis (Fe$_{igneous}$ + npOx) is the percentage of total Fe associated with blueberry-free basaltic soil at Meridiani Planum except for minor hematite, and the x-axis is the percentage of total Fe associated with jarosite. The plot shows that there is no meaningful difference in MB data obtained from undisturbed and RATed surfaces. In Figure 28.8b, where the y-axis is the SO$_3$ concentration by APXS, there is a clear offset in SO$_3$ concentrations, with RATed surfaces on average having elevated SO$_3$ concentrations compared to undisturbed surfaces. The offset is interpreted as a deeper sampling depth for MB compared to APXS-class

instruments, and it underscores the science value of RATting (or at least brushing) to obtain reliable rock chemistry in the presence of dust/soil coatings. On the basis of laboratory experiments, a layer of basaltic dust >3 mm thick is required to completely mask MB detection (14.4 keV) of underlying substrate (see **28.2 Instrument and Methods**).

Therefore, an important feature of MB is that it can "see through" thin layers of dust with no significant difference between undisturbed and brushed surfaces registered in spectra. More substantial layers of dust and weathering rinds or coatings do register in the spectra. Although not extensively investigated to date, the standard 14.4 keV gamma-ray spectra and the 6.4 keV X-ray spectra simultaneously acquired by the MIMOS II instrument can provide information on layer thickness. The difference in energy results in different penetration depths as a result of greater attenuation of lower energy radiation, and the difference allowed the successful identification and characterization of coatings such as on the rock Mazatzal in Gusev Crater (e.g., Fleischer *et al.*, 2008).

28.6 Summary

The Mössbauer spectrometers on the MER rovers provided first order information on the mineralogical composition, diversity, and oxidation state of igneous materials and their mineralogical alteration products. A total of 16 Fe-bearing phases were identified. At Gusev Crater, two major basaltic lithologies were identified: one with olivine and pyroxene and the other with pyroxene, variable olivine, and magnetite as the dominant Fe-bearing phases. Basaltic soil mineralogically similar to the olivine-pyroxene lithology but with variable proportions of npOx (associated with bright martian dust) was present throughout *Spirit's* traverse. The Columbia Hills of Gusev Crater are strongly altered compared to the Gusev plains and are characterized by a variety of Fe^{3+} bearing alterations products including npOx, goethite, hematite, and Fe^{3+}-bearing sulfate. An outcrop with Fe^{2+}-bearing carbonate was also detected in the Columbia Hills. This diversity in alteration products is a manifestation of a variety of alteration processes ranging from circum-neutral (goethite and carbonate) to acid-sulfate (Fe^{3+}-sulfate). The assemblage of Fe-bearing minerals is very different at Meridiani Planum, because the bedrock is dominated by the Fe^{3+}-bearing minerals hematite, jarosite, and an unassigned Fe^{3+}-bearing phase. Basaltic soil similar to the olivine-pyroxene soil at Gusev Crater is present on outcrop surfaces, both with and without admixed hematite concretions winnowed from the outcrop. Rocks that litter the Meridiani outcrop surface are interpreted as meteorites by the presence of kamacite and/or troilite or as indigenous basaltic ejecta from impacts into the martian surface by the absence of those phases. MB instruments can obtain mineralogical information on rock surfaces in the presence of dust coatings which would compromise chemical measurements by APXS-class instruments.

References

Ashley, J. W., M. P. Golombek, P. R. Christensen, S. W. Squyres, T. J. McCoy, C. Schröder, I. Fleischer, J. R. Johnson, K. E. Herkenhoff, and T. J. Parker (2011), Evidence for mechanical and chemical alteration of iron-nickel meteorites on Mars: Process insights for Meridiani Planum, *J. Geophys. Res.*, *116*(E7), E00F20, doi:10.1029/2010JE003672.

Arvidson, R. E., S. W. Squyres, R. C. Anderson, J. F. Bell III, J. Brückner, N. A. Cabrol, *et al.* (2006), Overview of the Spirit Mars Exploration Rover Mission to Gusev Crater: Landing Site to Backstay Rock in the Columbia Hills, *J. Geophys. Res.*, *111*, E02S01, doi:10.1029/2005JE002499.

Arvidson, R. E., S. Ruff, R. V. Morris, D. W. Ming, L. Crumpler, A. Yen, *et al.* (2008), Spirit Mars Exploration Rover mission to Gusev Crater, Columbia Hills: Mission overview and selected results from Cumberland Ridge to Home Plate, *J. Geophys. Res.*, *113*, E12S33, doi:10.1029/2008JE003183.

Arvidson, R. E., J. W. Ashley, J. F. Bell III, M. Chojnacki, J. Cohen, T. E. Economou, *et al.* (2010), Opportunity Mars Rover Mission: Overview and selected results from Purgatory Ripple to traverses to Endeavour Crater, *J. Geophys. Res.*, *116*, E00F15, doi:10.1029/2010JE003746.

Arvidson, R. E., J. F. Bell III, P. Belutta, N. A. Cabrol, J. G. Catalano, J. Cohen, *et al.* (2010), Spirit Mars rover mission: Overview and selected results from the northern Home Plate winter haven to the side of Scamander Crater, *J. Geophys. Res.*, *115*, E00F03, doi:10.1029/2010JE003633.

Bancroft, G. M. (1973), *Mössbauer Spectroscopy. An Introduction for Inorganic Chemists and Geochemists*, McGraw Hill, New York.

Burns, R. G., and T. C. Solberg (1990), ^{57}Fe-bearing Oxide, Silicate, and Aluminosilicate Minerals, Crystal Structure Trends in Mössbauer Spectra, in *Spectroscopic Characterization of Minerals and Their Surfaces*, edited by L. M. Coyne, S. W. S. McKeever and D. F. Blake, pp. 262-283, American Chemical Society, Washington, D. C.

Clark, B. C., R. V. Morris, S. M. McLennan, R. Gellert, B. Jolliff, A. H. Knoll, *et al.* (2005), Chemistry and mineralogy of outcrops at Meridiani Planum, *Earth Planet. Sci. Lett.*, *240*, 73-94.

Clark, B. C., R. E. Arvidson, R. Gellert, R. V. Morris, D. W. Ming, L. Richter, *et al.* (2007), Evidence for montmorillonite or its compositional equivalent in the Columbia Hills, Mars, J. Geophys. Res., 112, E06S01, doi:10.1029/2006JE002756.

De Grave, E., and A. Van Alboom (1991), Evaluation of ferrous and ferric Mössbauer fractions, *Phys. Chem. Minerals*, *18*, 337-342.

Dyar, M. D., and E. C. Sklute (2018), Chapter 7: Mossbauer Spectroscopy: Theory and Laboratory Spectra of Geologic Materials, This Book.

Dyar, M. D., E. Breves, E. Jawin, G. Marchand, M. Nelms, V. O'Connor, S. Peel, Y. Rothstein, E. C. Sklute, and M. D. Lane (2013), Mössbauer parameters of iron in sulfate minerals, *American Mineralogist*, *98*(11-12), 1943-1965.

Dyar, M. D., E. R. Jawin, E. Breves, G. Marchand, M. Nelms, M. D. Lane, S. A. Mertzman, D. L. Bish, and J. L. Bishop (2014), Mössbauer parameters of iron in phosphate minerals: Implications for interpretation of martian data, *American Mineralogist*, *99*, 914-942.

Fleischer, I., G. Klingelhöfer, C. Schröder, R.V. Morris, M. Hahn, D. Rodionov, R. Gellert, and P.A. de Souza Jr. (2008), Depth selective Mössbauer Spectroscopy: Analysis and

simulation of 6.4 keV and 14.4 keV spectra obtained from rocks at Gusev Crater, Mars, and layered laboratory samples, *J. Geophys. Res., 113*, E06S21, doi:10.1029/2007JE003022.

Fleischer, I., D. G. Agresti, G. Klingelhöfer, and R. V. Morris (2010a), Distinct hematite populations from simultaneous fitting of Mössbauer spectra from Meridiani Planum, Mars, *J. Geophys. Res., 115*, E00F06, doi:10.1029/2010JE003622.

Fleischer, I., J. Bruckner, C. Schroeder, W. Farrand, E. Treguier, R. V. Morris, *et al.* (2010b), Mineralogy and chemistry of cobbles at Meridiani Planum, Mars, investigated by the Mars Exploration Rover Opportunity, *J. Geophys. Res., 115*, E00F05, doi:10.1029/2010JE003621.

Fleischer, I., C. Schröder, G. Klingelhöfer, J. Zipfel, R. V. Morris, J. W. Ashley, R. Gellert, S. Wehrheim, and S. Ebert (2011), New insights into the mineralogy and weathering of the Meridiani Planum meteorite, Mars, *Meteoritics & Planetary Science, 46*(1), 21-34.

Graff, T. G., R. V. Morris, and P. R. Christensen (2001), Effects of palagonitic dust coatings on thermal emission spectra of rocks and minerals: Implications for mineralogical characterization of the Martian surface by MGS-TES, *Lunar and Planetary Science Conference, XXXII*, Abstract 1899.

Gütlich, P., and C. Schröder (2012), Mössbauer Spectroscopy. In: *Methods in Physical Chemistry*, edited by R. Schäfer and P.C. Schmidt, Wiley-VCH, pp. 351-389, doi:10.1002/9783527636839.ch11.

Gütlich, P., E. Bill, and A. X. Trautwein (2011), *Mössbauer Spectroscopy and Transition Metal Chemistry*, Springer Berlin Heidelberg, doi:10.1007/978-3-540-88428-6.

Hausrath, E. M., D. C. Golden, R. V. Morris, D. G. Agresti, and D. W. Ming (2013), Acid sulfate alteration of fluorapatite, basaltic glass and olivine by hydrothermal vapors and fluids: Implications for fumarolic activity and secondary phosphate phases in sulfate-rich Paso Robles soil at Gusev Crater, Mars, *J. Geophys. Res. Planets, 118*(1), 1-13.

Hawthorne, F. C., (1988), *Mössbauer Spectroscopy*, 255-340 pp., Mineralogical Society of America.

Klingelhöfer, G., R. V. Morris, B. Bernhardt, D. Rodionov, P. A. de Souza Jr., S. W. Squyres, *et al.* (2003), Athena MIMOS II Mössbauer spectrometer investigation, *J. Geophys. Res., 108*, 8067, doi: 10.1029/2003JE002138.

Klingelhöfer, G., R. V. Morris, B. Bernhardt, C. Schröder, D. S. Rodionov, P. A. de Souza Jr., *et al.* (2004), Jarosite and hematite at Meridiani Planum from Opportunity's Mössbauer spectrometer, *Science, 306*, 1740-1745.

Klingelhöfer, G., E. DeGrave, R. V. Morris, A. Van Alboom, V. G. de Resende, P. A. De Souza, D. Rodionov, C. Schröder, D. W. Ming, and A. Yen (2005), Mössbauer spectroscopy of Mars: goethite in the Columbia Hills at Gusev Crater, *Hyperfine Interact*, doi:10.1007/s10751-006-9329-y.

Lane, M. D., M. D. Dyar, and J. L. Bishop (2004), Spectroscopic evidence for hydrous iron sulfate in the Martian soil, *Geophys. Res. Lett., 31*, L19702, doi:10.1029/2004GL021231.

Lane, M. D., J. L. Bishop, M. D. Dyar, P. L. King, M. Parente, and B. C. Hyde (2008), Mineralogy of the Paso Robles soils on Mars, *Amer. Mineral., 93*, 728-739.

McCammon, C. (1995), *Mössbauer spectroscopy of minerals*, 332-347 pp., American Geophysical Union, Washington DC.

McSween, H. Y., S. W. Ruff, R. V. Morris, R. Gellert, G. Klingelhöfer, P. R. Christensen *et al.* (2008), Mineralogy of volcanic rocks in Gusev Crater, Mars: Reconciling Mössbauer,

Alpha Particle X-Ray Spectrometer, and Miniature Thermal Emission Spectrometer spectra, *J. Geophys. Res.* 113, E06S04, doi:10.1029/2007JE002970.

Morris, R. V., D. C. Golden, J. F. Bell III, and H. V. Lauer Jr. (1995), Hematite, pyroxene, and phyllosilicates on Mars: Implications from oxidized impact melt rocks from Manicouagan Crater, Quebec, Canada, *J. Geophys. Res.*, *100*, 5319-5328.

Morris, R. V., D. C. Golden, D. W. Ming, T. D. Shelfer, L. C. Jorgensen, J. F. Bell III, T. G. Graff, and S. A. Mertzman (2001a), Phyllosilicate-poor palagonitic dust form Mauna Kea Volcano (Hawaii): A mineralogical analogue for magnetic martian dust?, *J. Geophys. Res.*, *106*, 5057-5083.

Morris, R. V., T. G. Graff, T. D. Shelfer, and J. F. Bell III (2001b), Effect of palagonitic dust coatings on visible, near-IR and Mössbauer spectra of rocks and minerals: Implications for mineralogical remote sensing of Mars, *Lunar and Planetary Science Conference*, *XXXII*, Abstract 1912.

Morris, R. V., and G. Klingelhöfer (2008), *Chapter 15. Iron Mineralogy and Aqueous Alteration on Mars from the MER Mössbauer Spectrometers*, Cambridge University Press.

Morris, R. V., G. Klingelhöfer, B. Bernhardt, C. Schröder, D. S. Rodionov, P. A. de Souza Jr., *et al.* (2004), Mineralogy at Gusev Crater from the Mössbauer spectrometer on the Spirit rover, *Science, 305*, 833-836.

Morris, R. V., S. V. Ruff, R. Gellert, D. W. Ming, R. E. Arvidson, B. C. Clark, *et al.* (2010), Identification of carbonate-rich outcrops on Mars by the Spirit rover, *Science,* published online 3 June 2010, 2010.1126/science.1189667.

Morris, R. V., G. Klingelhöfer, C. Schröder, D. S. Rodionov, A. Yen, D. W. Ming, *et al.* (2006), Mössbauer mineralogy of rock, soil, and dust at Gusev Crater, Mars: Spirit's journey through weakly altered olivine basalt on the Plains and pervasively altered basalt in the Columbia Hills, *J. Geophys. Res.*, *111*, E02S13, doi:10.1029/2005JE002584.

Morris, R. V., G. Klingelhöfer, C. Schröder, D. S. Rodionov, A. Yen, D. W. Ming, *et al.* (2006), Mössbauer mineralogy of rock, soil, and dust at Meridiani Planum, Mars: Opportunity's journey across sulfate-rich outcrop, basaltic sand and dust, and hematite lag deposits, *J. Geophys. Res.*, *111*, E12S15, doi:10.1029/2006JE002791.

Morris, R. V., G. Klingelhöfer, C. Schröder, I. Fleischer, D. W. Ming, A. S. Yen, *et al.* (2008), Iron mineralogy and aqueous alteration from Husband Hill through Home Plate at Gusev Crater, Mars: Results from the Mössbauer instrument on the Spirit Mars Exploration Rover, *J. Geophys. Res.*, *113*, E12S42, doi:10.1029/2008JE003201.

Morris, R. V., J. G. Catalano, G. Klingelhoefer, C. Schröder, R. Gellert, B. C. Clark, D. W. Ming, A. S. Yen, R. E. Arvidson, B. A. Cohen, I. Fleischer, T. J. McCoy, D. W. Mittlefehldt, and S. W. Squyres (2018), Acid sulfate alteration at Gusev Crater and across Mars: Anoxic high-silica residues and oxic precipitation of ferric-bearing sulfate salts, *J. Geophys. Res.*, to be submitted.

Schröder, C., D. S. Rodionov, T. J. McCoy, B. L. Jolliff, R. Gellert, L. R. Nittler, *et al.* (2008), Meteorites on Mars observed with the Mars Exploration Rovers, *J. Geophys. Res.*, *113*, E06S22, doi:10.1029/2007JE002990.

Schröder, C., K. E. Herkenhoff, W. H. Farrand, J. E. Chappelow, W. Wang, L. R. Nittler, J. W. Ashley, I. Fleischer, R. Gellert, and M. P. Golombek (2010), Properties and distribution of paired candidate stony meteorites at Meridiani Planum, Mars, *J. Geophys. Res.*, *115*(E7), E00F09, doi:10.1029/2010JE003616.

Schröder, C., P. A. Bland, M. P. Golombek, J. W. Ashley, N. H. Warner, and J. A. Grant (2016), Amazonian chemical weathering rate derived from stony meteorite finds at Meridiani Planum on Mars, *Nature Communications*, *7*, 13459 doi:10.11038/ncomms13459.

Squyres, S. W., R. E. Arvidson, E. T. Baumgartner, J. F. Bell III, P. R. Christensen, S. Gorevan, *et al.* (2003), The Athena Mars rover science investigation, *J. Geophys. Res.*, *108*, 8062, doi:8010.1029/2003JE002121.

Squyres, S. W., R. E. Arvidson, J. F. Bell III, J. Brückner, N. A. Cabrol, W. Calvin, *et al.* (2004), The Spirit rover's Athena science investigation at Gusev Crater, Mars, *Science*, *305*, 794-799.

Squyres, S. W., R. E. Arvidson, J. F. Bell III, J. Brückner, N. A. Cabrol, W. Calvin, *et al.* (2004), The Opportunity rover's Athena science investigation at Meridiani Planum, Mars, *Science*, *306*, 1698-1703.

Squyres, S. W., R. E. Arvidson, D. Bollen, J. F. Bell III, J. Brückner, N. A. Cabrol, *et al.* (2006), Overview of the Opportunity Mars Exploration Rover Mission to Meridiani Planum: Eagle Crater to Purgatory Ripple, *J. Geophys. Res.*, *111*, E12S12, doi:10.1029/2006JE002771.

Squyres, S. W., R. E. Arvidson, S. Ruff, R. Gellert, R. V. Morris, D. W. Ming, *et al.* (2008), Detection of silica-rich deposits on Mars, *Science*, *320*, 1063-1067.

Squyres, S. W., A. H. Knoll, R. E. Arvidson, J. W. Ashley, J. F. Bell III, W. M. Calvin, *et al.* (2009), Exploration of Victoria Crater by the Rover Opportunity, *Science*, *324*, 1058-1061.

Yen, A. S., R. Gellert, C. Schröder, R. V. Morris, J. F. Bell III, A. T. Knudson, *et al.* (2005), An integrated view of the chemistry and mineralogy of Martian soils, *Nature, 436|7, doi:10.1038/nature03637*.

Yen, A. S., R. V. Morris, B. C. Clark, R. Gellert, A. T. Knudson, S. Squyres, *et al.* (2008), Hydrothermal processes at Gusev Crater: An evaluation of Paso Robles class soil, *J. Geophys. Res.*, *113*, E06S10, doi:10.1029/2007JE002978.

Yoshida, Y., and G. Langouche (2013), *Mössbauer Spectroscopy*, Springer Berlin Heidelberg, doi:10.1007/978-3-642-32220-4.

Zipfel, J., C. Schröder, B. L. Jolliff, R. Gellert, K. E. Herkenhoff, R. Rieder, *et al.* (2011), Bounce Rock – A Shergottite-like basalt encountered at Meridiani Planum, Mars, *Meteorit. Planet. Sci.*, *46*, DOI: 10.1111/J.1945-5100.2010.01127.X.

_____